Master's thesis

NTNU
Norwegian University of Science and Technology
Faculty of Natural Sciences
Department of Physics

Johan Besse Stamnes

Monte Carlo Simulations of Titanium-Aluminium Alloys based on the Cluster Expansion Method

Master's thesis in Applied Physics and Mathematics
Supervisor: Jaakko Akola
June 2019

NTNU
Norwegian University of
Science and Technology

Johan Besse Stamnes

Monte Carlo Simulations of Titanium-Aluminium Alloys based on the Cluster Expansion Method

Master’s thesis in Applied Physics and Mathematics
Supervisor: Jaakko Akola
June 2019

Norwegian University of Science and Technology
Faculty of Natural Sciences
Department of Physics

NTNU
Norwegian University of
Science and Technology

Abstract

Titanium-aluminium alloys in the range up to 50% aluminium have been studied with Monte Carlo simulations using a cluster expansion model based on density functional theory calculations. The calculator used is the open-source code GPAW, with the Perdew-Burke-Ernzerhof exchange-correlation energy functional. Several calculations of physical properties of pure titanium are performed to evaluate and validate the execution of the density functional theory calculations. The energies for a set of structures of varying titanium-aluminium composition on a hexagonal close-packed lattice were calculated and used to develop a cluster expansion model for the alloy. The clusters and effective cluster interactions of this model are briefly interpreted before used to perform Monte Carlo simulations on larger structures with the Metropolis-Hastings algorithm. Simulations are performed in both the canonical and the semi-grand canonical ensemble. The enthalpy of formation for the alloy is calculated up to 50% aluminium, and a Ti3Al crystal structure phase is identified.

Sammendrag

Titan-aluminium legeringer opp til 50% aluminium har blitt studert ved hjelp av Monte Carlo-simuleringer som bruker en klynge-ekspansjonsmodell basert på utregninger gjort med tetthetsfunksjonalteori. Kalkulatoren som er brukt, er opensource-koden GPAW sammen med Perdew-Burke-Ernzerhof funksjonalet. Flere utregninger for rent titans fysiske egenskaper har blitt gjort for å evaluere og validere utførelsen av tetthetsfunksjonalteoriutregningene. Energiene til et sett med strukturer med varierende sammensetning av titan og aluminium i heksagonalt tettpakket gitterstruktur ble regnet ut og brukt til å lage en klynge-ekspansjonsmodell for legeringen. Klyngene og de effektive klyngeinteraksjonene i denne modellen er kjapt diskutert før de er brukt til å kjøre Monte Carlo-simuleringer på større strukturer med Metropolis-Hastings algoritmen. Simuleringene er gjort i både det kanoniske og det semi-store kanoniske ensemblet. Formeringsentalpien for legeringen er utregnet opp til 50% aluminium, og en fase med Ti3Al-krystallstruktur ble funnet.

Preface

This Master thesis was written during the spring of 2019 and marks the end of my five-year Master of Science degree in Applied Physics and Mathematics at the Norwegian University of Science and Technology. In this thesis, the titanium-aluminium alloy is investigated with computational methods. I would like to thank my supervisor, Jaakko Akola, for supplying me with, and guiding me through an interesting and challenging topic for computer simulations. I would also like to thank PhD Candidate David Kleiven, for helping me out with the implementation of all the computational methods. Lastly, I would like to thank my fellow physics student, Rasmus André Tranås, for numerous productive discussions.

List of Figures

1.1 The phase diagram for the titanium-aluminium alloy [2]. 3

2.1 Schematic visualisation of the two structures with lattice vectors. The basis atoms are represented by white spheres. 7

7.1 Convergence of energy per atom as the cutoff energy is increased. These calculations are done with 10 k-points in each dimension. 32

7.2 Convergence of the energy per atom with an increasing number of k-points. On the x-axis, the number of k-points represents one dimension. The total number of k-points is therefore N^3 and $E_{cut} = 600$ eV. The 64-atom simulation converges very quickly, while the single atom is unstable at lower values of k-points. They converge to the same energy. 33

7.3 Simulating 64 titanium atoms in bcc structure for different lattice constants. The lowest energy is the lattice constant according to these simulations. 33

7.4 Band structure for bcc titanium. As expected for a metal, the bands cross over the Fermi level. 35

7.5 Bandstructure for hcp titanium. It has more bands close to the fermi level than its bcc counterpart. 36

7.6 Energy of a single titanium atom. As the size of the unit cell increases, the energy quickly converges towards the energy of an atom in free space. 36
7.7 The 63 atom structure used for finding the vacancy formation energy. The yellow arrow shows the location of the vacancy. . . 37
7.8 An evaluation of the CE predictions compared to the DFT calculations for all structures in the training set. 39
7.9 The DFT energies for the structures alongside the CE predictions plotted as enthalpy of formation. The points on the black line indicate favourable structures at that concentration. 40
7.10 The effective cluster interactions for each cluster in the model. Evidently, the zero and one atom cluster dominate. 41
7.11 ECIs without the zero and one atom cluster. 41
7.12 A selection of the most influential clusters. 42
7.13 Enthalpy of formation for titanium-aluminium for a range of energies. 43
7.14 Visualisation of the bulk at 25% and 50% concentration at 100 K from the calculations shown in figure 7.13. 44
7.15 Cooling down structures at different, constant chemical potentials. 45

Contents

Abstract **I**

Sammendrag **II**

Preface **III**

List of Figures **V**

Table of Contents **VII**

1 Introduction **1**

2 Crystal Structure **5**

2.1 Lattice 5
2.2 Body-Centered Cubic Structure 6
2.3 Hexagonal Close-Packed Structure 6
2.4 Reciprocal Lattice 7
2.5 Metals 8
2.5.1 Cohesive Energy 9
2.5.2 Vacancy Formation Energy 9
2.5.3 Enthalpy of Formation for Alloys 9
2.6 Fermi Level 10
2.7 Electronic Band Structure 11

3 Statistical Mechanics 13

3.1 Canonical Ensemble 13

3.2 Grand Canonical Ensemble 14

4 Density Functional Theory 15

4.1 The Schrödinger Equation 15

4.2 The Hartree-Fock Method 16

4.3 The Hohenberg-Kohn Theorems 17

4.4 Constrained Search Formulation 17

4.5 Exchange-Correlation functional 18

4.5.1 Local Density Approximation 18

4.5.2 Generalised-Gradient Approximation 18

5 Mathematical Methods 21

5.1 Cluster expansion 21

5.2 Monte Carlo 23

6 Computational Methods 25

6.1 ASE 25

6.2 DFT calculations with GPAW 25

6.3 Cluster Expansion with CLEASE 26

6.4 Monte Carlo Simulations with CEMC 29

7 Results and Discussion 31

7.1 Convergence Tests 31

7.2 Lattice Constants 32

7.3 Electronic Band Structure 34

7.4 Cohesive Energy 35

7.5 Vacancy Formation Energy 37

7.6 Optimising Structures for Cluster Expansion 38

7.7 Cluster Expansion 38

7.8 Monte Carlo Simulations 42

7.8.1 Canonical Ensemble 42

7.9 Grand Canonical Ensemble 44

8 Conclusion **47**

9 Future Work **49**

Chapter 1

Introduction

Metals are some of our most important materials as the combination of strength and moldability have made them contribute to many of the greatest technological endeavours of our species. From tools in the bronze age to spacecraft traversing the solar system, the art of refining metals and enhancing their properties has been of tremendous importance to the development of our society.

In the everlasting search for stronger and more durable materials, alloys of different metals provide a vast array of possible combinations to investigate. The way combining different metals change the properties is easy to observe on a macroscopic level, but understanding the microscopic structural changes and their implications requires advanced scientific methods. As experimental methods can be expensive, computer simulations are becoming increasingly useful for studying materials as computing methods are evolving and computer resources are increasing.

Titanium is a metal of high interest as its pure form already is a high strength and low weight material. By alloying with other metals, it can become even stronger. Titanium is actually one of the more abundant elements in the Earth's crust at ninth place [1], but it is rarely found in high concentrations and never in its pure form, resulting in high processing costs. Nonetheless, the expensive metal and its alloys have found their uses in a wide range of products, typically in industries of a high technological standard. Examples include jet engine parts in the aerospace industry and various components used in medical procedures. Titanium has, undoubtedly, found its way into common knowledge as a sort of wonder material.

In this thesis, aluminium will be investigated as an alloying element for titanium. The properties of the titanium-aluminium alloy will be investigated on an atomic scale through the use of computer simulations. Initially, the method used will be density functional theory (DFT), an approach to finding the electronic structure by expressing it as an electron density. Emphasis will be put on verifying that the results from the simulations are in agreement with experimental results, and pure titanium will be the subject for these tests. From DFT calculations of alloy structures, a cluster expansion (CE) model will be developed, which can then be used to execute Monte Carlo (MC) simulations for the alloy. The focus will be on the titanium-rich side of the phase diagram shown in figure 1.1. The alloy simulations will be performed with the hexagonal close-packed (hcp) lattice as this is the structure of pure titanium (αTi) at low temperatures. Pure aluminium has a face-centered cubic structure, an since the MC simulations used in this thesis are not able to treat multiple crystal structures at the same time, the simulations are kept below 50% aluminium. In addition, the body-centered cubic (bcc) structure will be used in a few calculations to compare results with calculations for hcp. It is of interest to see if the crystalline phases Ti3Al and TiAl in the phase diagram can be replicated by computer simulations.

Starting with chapter 2, some concepts related to crystal structures will be explained, a field within solid state physics. This is followed by a brief presentation of the canonical and grand canonical ensemble from statistical mechanics in chapter 3. Density functional theory and exchange-correlation functionals are introduced in chapter 4, while the CE method and Monte Carlo simulations are introduced in chapter 5. Then, the computational methods are presented in chapter 6 before the results of multiple computer simulations of both pure titanium and the titanium-aluminium alloy are presented in chapter 7.

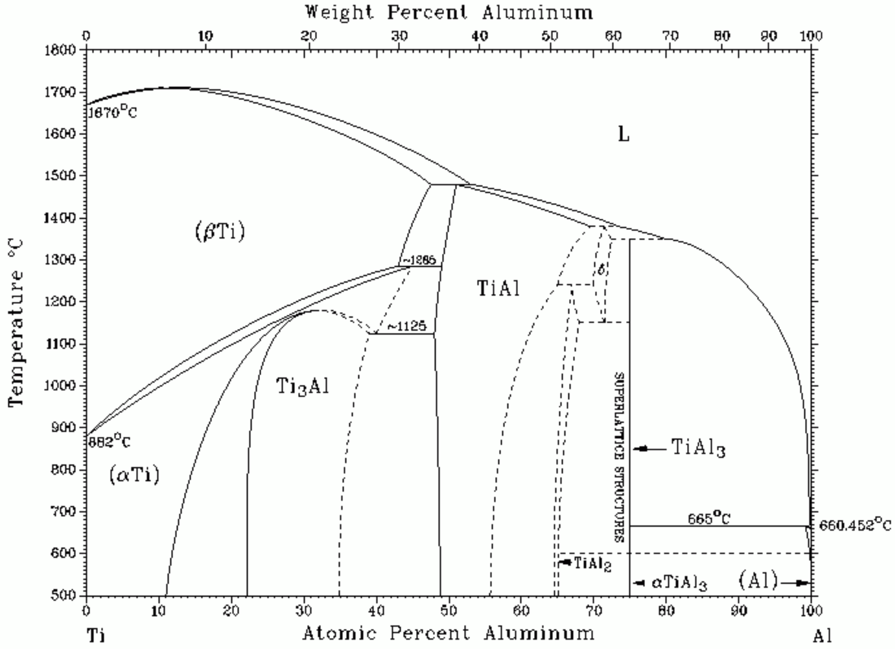

Figure 1.1: The phase diagram for the titanium-aluminium alloy [2].

Chapter 2

Crystal Structure

2.1 Lattice

A crystal structure can be described as an infinite repetition of a basis group of atoms [3]. The group is repeated on a lattice defined by three translation vectors. Moving any arbitrary integer number of vectors results in the lattice appearing the same in every direction.

$$\boldsymbol{r'} = \boldsymbol{r} + u_1\boldsymbol{a}_1 + u_2\boldsymbol{a}_2 + u_3\boldsymbol{a}_3 \tag{2.1}$$

where $\boldsymbol{a}_i$ are the lattice vectors and u_i are arbitrary integers. This describes how a position $\boldsymbol{r'}$ on a lattice is not unique, but equivalent to all other positions $\boldsymbol{r}$ given a translation on the lattice. If one point in space is defined as origo, all integer translations from this point constitute the lattice sites of the crystal. All sites are the reference point for a basis, which is identical at every site. In the simplest case, the basis is just a single atom, but it can be any number of different atoms at different positions

$$\boldsymbol{r}_j = x_j\boldsymbol{a}_1 + y_j\boldsymbol{a}_2 + z_j\boldsymbol{a}_3 \tag{2.2}$$

with $0 \leq x_j, y_j, z_j < 1$, meaning that the j'th atom is placed somewhere less than one translation vector away.

2.2 Body-Centered Cubic Structure

The *bcc* structure consists of a cube with one sphere in every corner and one in the centre, visualised in figure 2.1a. The translation vectors are

$$\boldsymbol{a}_1 = \big(\frac{a}{2}, \frac{a}{2}, -\frac{a}{2}\big) \quad \boldsymbol{a}_2 = \big(\frac{a}{2}, -\frac{a}{2}, \frac{a}{2}\big) \quad \boldsymbol{a}_3 = \big(-\frac{a}{2}, \frac{a}{2}, \frac{a}{2}\big). \tag{2.3}$$

This structure has a packing fraction of 0.68, meaning that closely packed spheres take up this fraction of the total volume.

2.3 Hexagonal Close-Packed Structure

The *hcp* structure is shown in figure 2.1b and is obtained by arranging spheres on a two-dimensional hexagonal lattice and stacking several of these on top of each other, called AB stacking. The layers are placed relative to each other so that every sphere has three equally distanced neighbours in the next layer. The translation vectors are

$$\boldsymbol{a}_1 = \big(\frac{a}{2}, \frac{\sqrt{3}a}{2}, 0\big) \quad \boldsymbol{a}_2 = \big(\frac{a}{2}, -\frac{\sqrt{3}a}{2}, 0\big) \quad \boldsymbol{a}_3 = \big(0, 0, c\big), \tag{2.4}$$

with two lattice constants a and c. It has a two-atom basis with the second atom in position $\boldsymbol{r} = \frac{1}{3}\boldsymbol{a}_1 + \frac{2}{3}\boldsymbol{a}_2 + \frac{1}{2}\boldsymbol{a}_3$. In an ideal hcp structure, the ratio between the lattice constants is fixed to $c = \frac{2\sqrt{6}}{3}a$. It then has a packing fraction of 0.74, the highest obtainable for hard spheres.

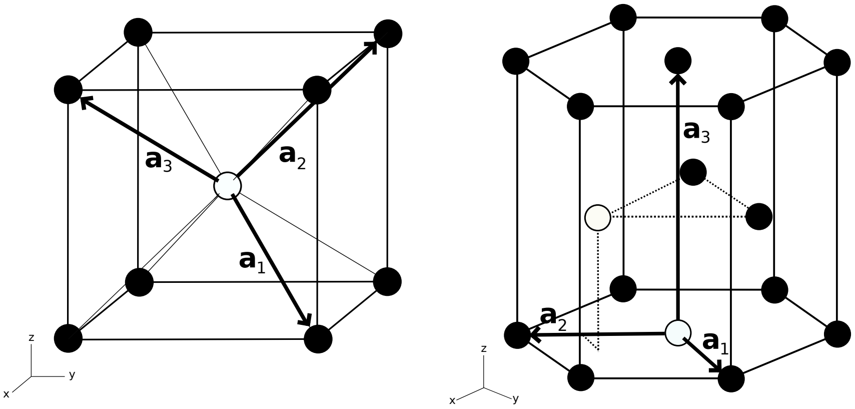

(a) Body-centered cubic **(b)** Hexagonal close-packed

Figure 2.1: Schematic visualisation of the two structures with lattice vectors. The basis atoms are represented by white spheres.

2.4 Reciprocal Lattice

The lattice of a crystal structure is an intuitive representation of the physical placements of atoms, but to study aspects linked closely to the periodicity of the structure, Fourier analysis provides more insight. A Fourier transform of the lattice is called the *Reciprocal Lattice*[3]. Like the real-space lattice, the reciprocal lattice is described by a set of vectors

$$\mathbf{G} = v_1\mathbf{b}_1 + v_2\mathbf{b}_2 + v_3\mathbf{b}_3 \tag{2.5}$$

where v_i is an integer. This set of vectors has to fulfil the condition

$$n(\mathbf{r}) = \sum_{\mathbf{G}} n_{\mathbf{G}} \exp\left(i\mathbf{G}\cdot\mathbf{r}\right) \tag{2.6}$$

for any translation $\mathbf{T} = u_1\boldsymbol{a}_1 + u_2\boldsymbol{a}_2 + u_3\boldsymbol{a}_3$ on the lattice. Here, $n_{\mathbf{G}}$ is a set of Fourier coefficients and $n(\mathbf{r})$ is a physical property of the crystal, for example the electron density. The set of vectors $\mathbf{G}$ can be found from the lattice vectors:

$$\mathbf{b}_1 = 2\pi\frac{\mathbf{a}_2 \times \mathbf{a}_3}{\mathbf{a}_1 \cdot \mathbf{a}_2 \times \mathbf{a}_3} \quad \mathbf{b}_2 = 2\pi\frac{\mathbf{a}_3 \times \mathbf{a}_1}{\mathbf{a}_1 \cdot \mathbf{a}_2 \times \mathbf{a}_3} \quad \mathbf{b}_3 = 2\pi\frac{\mathbf{a}_1 \times \mathbf{a}_2}{\mathbf{a}_1 \cdot \mathbf{a}_2 \times \mathbf{a}_3}. \tag{2.7}$$

In the real space, vectors on the lattice describe positions and the unit of a vector is length. In the reciprocal space, vectors have the unit 1/length and describe waves with a certain direction and wave number. Since electrons quantum mechanically are waves within the crystal structure, vectors in the reciprocal space is a powerful tool for studying their behaviour. Bloch's theorem states that a solution to the Schrödinger equation in a periodic potential must be

$$\psi(\mathbf{r}) = u(\mathbf{r}) \exp(i\mathbf{k} \cdot \mathbf{r}) \tag{2.8}$$

with $u(\mathbf{r})$ being a potential with the same period as the crystal structure and $\mathbf{k}$ is a wave vector. This means that k-vectors in the reciprocal space are very useful for describing electrons in crystal structures.

An essential concept in reciprocal space is the *Brillouin zone*. It can be defined as a volume around a reciprocal lattice point where no part of the volume is closer to any other lattice point. Since a translation $\mathbf{G}$ results in the lattice looking the same in all directions, the behaviour of electrons can be described by looking at just one Brillouin zone.

2.5 Metals

The electrons in an atom's outermost shell are called valence electrons and are one of the causes for interaction between atoms. For certain atoms, lower energy is obtained by freely sharing the valence electrons within a bulk of atoms. This is called metal bonding and is better described as positive ions floating in a sea of electrons. No neighbouring ions are directly bound to each other, more just restricted by the electric field caused by the sea of electrons and neighbouring ions. As a consequence, the energy required for rearrangement of the structure is low compared to other types of solids. This leads to a higher chance of relaxing to the ground state, rendering metals a solid likely to form crystals.

2.5.1 Cohesive Energy

The cohesive energy is the difference in energy between a single atom in free space and the same atom in a crystal structure [4]. It is thereby a measure of how well the atoms "cling together" in a given structure. It can be defined as

$$E_c = E_s - \frac{E_b}{N} \tag{2.9}$$

with E_s being the energy of a single atom in free space and E_b is the total energy of a bulk of N atoms. If E_c is positive, the energy per atom is lowered by being ordered in a crystal, meaning that this structure is preferable.

2.5.2 Vacancy Formation Energy

Another way of measuring how well atoms in a metal are bound together is the vacancy formation energy. An atom is removed from the fully occupied lattice, resulting in a slightly different ordering of the neighbouring atoms. The new structure is not ideal for the electrons in the area, and the energy per atom is increased. The vacancy formation energy [5] can be described by

$$E_{vf} = E_v - \frac{N-1}{N} E_b \tag{2.10}$$

where E_v is the total energy of the bulk of atoms with a vacancy.

2.5.3 Enthalpy of Formation for Alloys

Due to the nature of the metallic bonding and its sea of electrons, different elements may very well coexist within the same structure, called an alloy. The structure of an alloy is not necessarily ordered, but at the right concentrations of components and thermal processing, it can form crystals. Regardless of structure, the mixing of different elements will change the enthalpy of the system. Enthalpy is defined as

$$H = U + pV \tag{2.11}$$

where U is the internal energy, p is the pressure and V is the volume. The enthalpy of formation is the change in enthalpy from the pure, separated elements to the mixed alloy, expressed as

$$H_{formation} = \sum H_{alloy} - \sum H_{start}. \tag{2.12}$$

Consider a binary alloy in the special case where the pressure $p = 0$. The enthalpy is then the same as the internal energy and in this case the enthalpy of formation is

$$H_{formation} = E_{alloy} - C_a E_a - C_b E_b \tag{2.13}$$

where E_{alloy} is the average internal energy per atom in the alloy and E_a and E_b is the internal energy per atom for the pure crystal of element a and b. The atomic concentration C is expressed as a fraction so that $C_a + C_b = 1$. Enthalpy of formation as a function of concentration is an intuitive insight into the nature of the alloy. Positive values mean that the different elements have a lower total energy by staying separated, and no alloy will form. Negative values represent situations where it is energetically beneficial for the elements to mix, with the minimum enthalpy of formation representing the most stable alloy.

2.6 Fermi Level

As electrons are fermions, they obey the Pauli exclusion principle [3, p. 56] stating that two fermions may not occupy the same quantum state. In an N-electron system in the ground state, the energy of the topmost filled level is called the Fermi energy. At absolute zero temperature, all possible energy states below this energy are occupied. If the temperature is increased, electrons can move to higher states, leaving some lower states vacant. The Fermi-Dirac distribution gives the probability that an energy state ϵ is occupied as

$$f(\epsilon) = \frac{1}{\exp[(\epsilon - \mu)/k_B T] + 1} \tag{2.14}$$

where T is the temperature and μ is the Fermi level. At the state where $\epsilon = \mu$, the probability of occupancy is $\frac{1}{2}$, and this defines the Fermi level. It is also apparent that at zero Kelvin the probability is 1 for finding occupied states below the Fermi level and 0 above.

2.7 Electronic Band Structure

The behaviour of electrons in a solid can be studied by looking at the electronic band structure. Energy is plotted against the wave vector $\mathbf{k}$ to show the allowed energies in the structure. The energy band below the Fermi level in the diagram is called the valence band, and the band over is called the conduction band. A material's ability to conduct electricity is determined by the ability for electrons to move from the valence band to the conduction band. The electrons are then free to move between the ion cores and conduct electricity. A vacancy in the valence band will also contribute to the conductivity as the "hole" can jump between ions. In a metal, there will be a continuous line across the Fermi level, allowing electrons to move from the valence band to the conduction band without the supply of external energy. The lack of a continuous line from lower to higher energy is called a band gap.

As mentioned earlier, it is sufficient to plot only one Brillouin zone as the plotted lines originating in the adjacent zones carry on into that zone for the higher energies. Also, since $\mathbf{k}$ is a vector in reciprocal space, it is common to plot the energy along a path of high-symmetry axes in the Brillouin zone.

Chapter 3

Statistical Mechanics

In this chapter, a few concepts from the field of statistical mechanics are briefly introduced, based on reference [6].

3.1 Canonical Ensemble

Consider a system consisting of a collection of particles described by a Hamiltonian H. The system is allowed to exchange energy with the surroundings, but the number of particles and the volume they occupy is constant. The canonical ensemble is the collection of all possible states of this system. The temperature T is then a property of the system which is allowed to vary and determines the probability of occupying a specific state of the canonical ensemble. The probability is

$$P(E_i) = \frac{e^{-\beta E_i}}{Z} \tag{3.1}$$

where E_i is the energy of state i and β is defined as $1/k_B T$, employing the Boltzmann constant k_B. Z is the partition function defined as

$$Z = \sum_i e^{-\beta E_i} \tag{3.2}$$

which is a fundamental quantity in statistical mechanics. An important observation is that a lower temperature makes the lower energy states more probable while letting $T \to \infty$ results in all energy states having an equal probability of being occupied.

3.2 Grand Canonical Ensemble

In addition to allowing the exchange of energy with the surroundings, the grand canonical ensemble allows the exchange of particles. By introducing a chemical potential μ, the probability of state occupancy is

$$P(E_{i,N}) = \frac{e^{-\beta(E_{i,N} - \mu N)}}{\Theta} \tag{3.3}$$

with the particle number N and the grand canonical partition function

$$\Theta = \sum_{i,N} = e^{-\beta(E_{i,N} - \mu N)}. \tag{3.4}$$

With the grand canonical ensemble allowing the system to change its composition of particles, a wider range of applications is opened up for this formalism, for example, the adsorption of particles into a material.

Chapter 4

Density Functional Theory

DFT is a computational method for modelling the electronic structure of many-body systems. Instead considering every electron as a particle, it utilises the electron density in the calculations. Quantum mechanical effects are added by applying a functional, a function of a function, to the electron density. In this section, the theory behind it will be explained further.

4.1 The Schrödinger Equation

By solving the many-body Schrödinger equation,

$$\hat{H}\psi = \left[-\frac{\hbar}{2m} \sum_{i=1}^{N} \nabla_i^2 + \sum_{i=1}^{N} V(\boldsymbol{r}_i) + \sum_{i=1}^{N} \sum_{j<i} U(\boldsymbol{r}_i, \boldsymbol{r}_j) \right] \psi = E\psi, \tag{4.1}$$

an exact solution to a system can be found. It links the many-body wave function ψ to the energy E with the Hamiltonian $\hat{H}$. Here, m is mass and $\hbar$ is the reduced Planck constant. $V(\boldsymbol{r}_i)$ is the electron-nucleus attraction energy and $U(\boldsymbol{r}_i, \boldsymbol{r}_j)$ is the electron-electron repulsion energy. As the equation considers all particles and the interactions between each and everyone, calculations become very complex for larger systems.

4.2 The Hartree-Fock Method

By making some approximations, the complexity can be greatly reduced. The Hartree-Fock method [7][8] approximates a wave function for a system by approaching the electron-electron interactions differently. A system of electrons can be described by

$$\psi(\mathbf{x}_1, \mathbf{x}_2 \cdots \mathbf{x}_N) = \psi(\mathbf{x}_1)\psi(\mathbf{x}_2)\cdots\psi(\mathbf{x}_N), \tag{4.2}$$

making each electron's wave independent of the other. A problem with this approximation is that it violates the Pauli exclusion principle because it does not satisfy the anti-symmetry principle. For two electrons this can be solved with a wave function like this:

$$\psi(\mathbf{x}_1, \mathbf{x}_2) = \frac{1}{\sqrt{2}}\big[\psi_1(\mathbf{x}_1)\psi_2(\mathbf{x}_2) - \psi_1(\mathbf{x}_2)\psi_2(\mathbf{x}_1)\big]. \tag{4.3}$$

This can be generalised by using a determinant to account for systems of arbitrary size with

$$\psi = \frac{1}{\sqrt{N!}}\begin{vmatrix} \psi_1(\mathbf{x}_1) & \psi_2(\mathbf{x}_1) & \cdots & \psi_N(\mathbf{x}_1) \\ \psi_1(\mathbf{x}_2) & \psi_2(\mathbf{x}_2) & \cdots & \psi_N(\mathbf{x}_2) \\ \vdots & \vdots & \ddots & \vdots \\ \psi_1(\mathbf{x}_N) & \psi_2(\mathbf{x}_N) & \cdots & \psi_N(\mathbf{x}_N) \end{vmatrix} \tag{4.4}$$

called the Slater determinant. The variational theorem states that the energy calculated by the Hamiltonian is always an upper bound to the true energy of the system. This implies that by minimising the energy, the true solution is approached. Without further elaboration the Hartree-Fock equations can be used to find the solution and this method can be viewed as a predecessor to density functional theory.

4.3 The Hohenberg-Kohn Theorems

Hohenberg and Kohn formulated DFT as an exact theory of many-body systems. If the Hamiltonian can be written on the form

$$\hat{H} = -\frac{\hbar^2}{2m_e}\sum_i \nabla_i^2 + \sum_i V_{ext}(\mathbf{r_i}) + \frac{1}{2}\sum_{i\neq j}\frac{e^2}{|\mathbf{r}_i - \mathbf{r}_j|} \tag{4.5}$$

the following theorems apply [9]:

1. For any system of interacting particles in an external potential $V_{ext}(\mathbf{r})$, the potential $V_{ext}(\mathbf{r})$ is determined uniquely, except for a constant, by the ground state particle density $n_0(\mathbf{r})$.
2. A universal functional for the energy $E[n]$ in terms of the density $n(\mathbf{r})$ can be defined, valid for any external potential $V_{ext}(\mathbf{r})$. For any particular $V_{ext}(\mathbf{r})$, the exact ground state energy of the system is the global minimum value of this functional, and the density $n(\mathbf{r})$ that minimises the functional is the exact ground state density $n_0(\mathbf{r})$.

A consequence of this is that all properties of the system are entirely determined by the ground state density $n_0(\mathbf{r})$ and the functional E[n] is sufficient to determine the energy and density of the ground state.

4.4 Constrained Search Formulation

Levy and Lieb defined a way to search for the ground state by minimising the energy in two steps [9]. First, the energy is minimised among wave functions with the same density $n(\mathbf{r})$. The total energy of a wave function can be written as

$$E = \langle\psi|\hat{T}|\psi\rangle + \langle\psi|\hat{V}_{int}|\psi\rangle + \int d^3r V_{ext}(\mathbf{r})n(\mathbf{r}) \tag{4.6}$$

where $\hat{T}$ is the kinetic energy and V_{int} is the electron interactions. It can be minimised for a specific electron density with

$$E_{LL}[n] = F_{LL}[n] + \int d^3r V_{ext}(\mathbf{r})n(\mathbf{r}) + E_{II} \tag{4.7}$$

where E_{II} is the interaction energy of the nuclei and

$$F_{LL}[n] = \min_{\psi \to n(\mathbf{r})} \langle \psi | \hat{T} + \hat{V}_{int} | \psi \rangle \,. \tag{4.8}$$

$E_{LL}[n]$ is then a function of the electron density and the second step is then to minimise this function to arrive at the ground state.

4.5 Exchange-Correlation functional

Kohn and Sham proposed an approach where it is assumed that the ground state density of a many-body system, with all its interactions, is equal to that of a chosen non-interacting system [9]. This leads to the opportunity of incorporating all the difficult many-body terms into an *exchange-correlation functional* of the density. The remaining terms describe a non-interacting system which can be solved exactly. This functional is not known, but there are several approximate functionals that work very well in given situations.

4.5.1 Local Density Approximation

By assuming a slowly varying electron density, LDA approximates the exchange-correlation functional without the use of any gradients. The method can be generalised with

$$E_{xc}^{LDA}[n] = \int d^3 r n(\mathbf{r}) \epsilon_{xc}(n(\mathbf{r})). \tag{4.9}$$

where ϵ_{xc} is an approximation of the exchange-correlation energy of a homogeneous electron gas at the given density.

4.5.2 Generalised-Gradient Approximation

As suggested by the name, GGAs incorporate the gradient of the electron density as well. By calculating the exchange-correlation functional from both the electron density and its gradient, the computation time increases, but so does the accuracy of the results. Similarly to LDA, the method can be generalised as

$$E_{xc}^{GGA}[n] = \int d^3r n(\mathbf{r}) \epsilon_{xc}(n(\mathbf{r}), \nabla n(\mathbf{r})). \tag{4.10}$$

Chapter 5

Mathematical Methods

In this chapter, the two main mathematical methods used in this thesis work are presented.

5.1 Cluster expansion

The following is a theoretical description of the cluster expansion (CE) method. Its application to binary alloys will be elaborated in section 6.

Consider a structure consisting of N lattice sites where each site has one of two possible values. The structure can then have any configuration in the space of a vector

$$\boldsymbol{\sigma} = \{\sigma_1, \sigma_2, ..., \sigma_N\} \tag{5.1}$$

with the discrete variable $\sigma_i = \pm 1$. The scalar product of two functions $f(\sigma)$ and $g(\sigma)$ is defined as

$$\langle f, g \rangle = \frac{1}{2} \sum_{\sigma=\pm 1} f(\sigma) g(\sigma). \tag{5.2}$$

A complete orthonormal basis in the one-dimensional space spanned by the dicrete σ is given by the two polynomials

$$\varphi_0(\sigma) = 1 \tag{5.3a}$$

$$\varphi_1(\sigma) = \sigma \tag{5.3b}$$

of order 0 and 1 respectively. An orthonormal basis in the space spanned by vector $\boldsymbol{\sigma}$ is then given as characteristic functions made by all possible products of the polynomials given in Eq. 5.3:

$$\boldsymbol{\Phi}_\alpha(\boldsymbol{\sigma}_\alpha) = \prod_{i \in \sigma} \varphi_1(\sigma_i). \tag{5.4}$$

The scalar product of two functions $f(\boldsymbol{\sigma}_\gamma)$ and $g(\boldsymbol{\sigma}_\gamma)$ in the configurational space of cluster γ can be expressed as

$$\langle f, g \rangle = \frac{1}{2^{n_\gamma}} \sum_{\sigma_1 = \pm 1} \cdots \sum_{\sigma_n = \pm 1} f(\boldsymbol{\sigma}_\gamma) g(\boldsymbol{\sigma}_\gamma) \tag{5.5}$$

where n_γ is the number of sites in cluster γ. Consequently, the orthogonality of the characteristic functions is expressed as

$$\langle \boldsymbol{\Phi}_\alpha, \boldsymbol{\Phi}_\beta \rangle = \frac{1}{2^{n_\gamma}} \sum_{\sigma_1 = \pm 1} \cdots \sum_{\sigma_n = \pm 1} \boldsymbol{\Phi}_\alpha(\boldsymbol{\sigma}_\alpha) \boldsymbol{\Phi}_\beta(\boldsymbol{\sigma}_\beta) = \delta_{\alpha,\beta} \tag{5.6}$$

with α and β being subclusters of γ. From the characteristic functions, any property q that is a function of the configuration $\boldsymbol{\sigma}$ can be expanded as

$$q(\boldsymbol{\sigma}) = \sum_\alpha \boldsymbol{V}_\alpha \boldsymbol{\Phi}_\alpha \tag{5.7}$$

where $\boldsymbol{V}$ is the effective cluster interaction (ECI) given by

$$\boldsymbol{V}_\alpha = \langle \boldsymbol{\Phi}_\alpha, q \rangle. \tag{5.8}$$

5.2 Monte Carlo

Monte Carlo (MC) is a method that has a wide range of applicability and implementations. It is, in essence, a form of numerical integration in which finite summations are used to estimate definite integrals [10]. It is often used on problems where it is possible to calculate an exact answer, but such an answer is too computationally expensive to obtain. Typically, these problems involve a system where the space spanned by all possible states of the system is practically infinite. In the MC method, a much smaller portion of this space is explored by letting random numbers choose which states are computed. If applied correctly, high accuracy can be obtained despite the limited space of states being investigated. The uncertainty created by the probabilistic element of the method is handled by the law of large numbers. A simple example of a Monte Carlo simulation is to calculate π with a random number generator. This can be done by defining a square with an inscribed circle. The random number generator then produces coordinates within the square. By Pythagoras' law, it can be determined whether the coordinate lies inside or outside the circle. By simulating many coordinates, π can be estimated from the ratio between the coordinates inside and outside. The more coordinates are simulated, the more accurate the result becomes.

Chapter 6

Computational Methods

6.1 ASE

Atomic Simulation Environment [11] is a software package written in Python used for setting up atomic simulations. The simplicity of the Python language makes it a powerful tool for easy high-level management of complicated simulation software. In ASE, the objects of interest can be set up by, for example, placing atoms at different positions in space. The desired simulations can then be carried out by importing and calling other software packages. It includes its own database type, which is convenient for working with atom structures.

6.2 DFT calculations with GPAW

GPAW is a software package for doing DFT calculations, operated through the ASE interface. Calculations can be executed with different ways of describing wave functions, for example, on a real-space grid or atom-centered functions for orbitals. In this project, the mode for describing wave functions is set to plane waves. GPAW is based on the projector-augmented wave (PAW) method [12]. The wave function for a material is fairly smooth in the bonding region, but oscillates rapidly close to the nucleus. The required resolution to describe the wave function accurately near the nucleus is not efficient use of computer resources in the bonding region. The strategy of the PAW method is to divide the wave function into two parts, one part as a partial wave expansion inside a nucleus-centered sphere and an envelope function outside the spheres.

There are two main parameters to consider when optimising the computational accuracy and execution time. The cutoff energy $E_{cut} = \mathbf{G}_{cut}^2/2$ determines the maximum size of the reciprocal lattice vectors. The number of k-points determines the sampling of the Brillouin zone. As a rule of thumb, a higher number of k-points is needed for smaller systems as the reciprocal space needed to describe them accurately is inversely proportional to the real space size. Analogously, the Dirac delta function requires an infinite amount of frequencies to be expressed in Fourier space. There are also different exchange-correlation functionals to choose from. Here, the Perdew-Burke-Ernzerhof (PBE) functional is used which is a GGA.

6.3 Cluster Expansion with CLEASE

To do cluster expansion, the package CLEASE is used [13]. It is an addition to the ASE software with the aim of making CE easy to implement on DFT data. Optimised structures along with their total energies is the input which produces a set of clusters along with their corresponding effective cluster interactions. Now, the number of clusters is theoretically infinite, but by choosing only a few of the most important ones the required accuracy is achieved. Having fewer ECIs results in a lower computational cost for the MC simulations later on. In CLEASE, this is achieved by the method of compressive sensing [14] based on the l_1 norm, a case of the l_p norm

$$||\boldsymbol{x}||_p = \left(\sum_i |x_i|^p \right)^{1/p} \tag{6.1}$$

with $p = 1$ and where $\boldsymbol{x}$ is a vector. This case of the norm is called the Manhattan distance, whereas the l_2 norm is the Euclidean distance. By writing

Eq. 5.7 on matrix form

$$\boldsymbol{q} = \boldsymbol{\Phi} \boldsymbol{V} \tag{6.2}$$

the problem of finding the ECIs can be solved with linear regression based on the l_1 norm. Here, $\boldsymbol{q}$ is a vector where the ith element corresponds to the physical quantity of configuration $\boldsymbol{\sigma}_i$. The matrix $\boldsymbol{\Phi}$ consists of all the characteristic functions and $\boldsymbol{V}$ is a vector containing the ECIs.

One way of determining the ECIs in $\boldsymbol{V}$ is by the ordinary least squares method. This is done by minimising the residual sum of squared errors (RSS)

$$RSS = ||\boldsymbol{\Phi} \boldsymbol{V} - \boldsymbol{q}||_2^2 \tag{6.3}$$

which has the unique solution $\hat{\boldsymbol{V}}$ calculated by

$$\hat{\boldsymbol{V}} = \arg \min_{\boldsymbol{V}} ||\boldsymbol{\Phi} \boldsymbol{V} - \boldsymbol{q}||_2^2 = (\boldsymbol{\Phi}^T \boldsymbol{\Phi})^{-1} \boldsymbol{\Phi}^T \boldsymbol{q}. \tag{6.4}$$

This method has the drawback that it needs more configurations in the training set than the number of clusters being considered, limiting the possible number of sites in the clusters. It is also prone to overfitting, meaning that the ECIs are tuned to accurately predict the physical property $\boldsymbol{q}$ for the configurations in the training set, at the cost of losing predictive power for configurations outside the set. To counter these drawbacks, the regularisation term l_1 mentioned earlier is added to eq. 6.4 which becomes

$$\hat{\boldsymbol{V}} = \arg \min_{\boldsymbol{V}} ||\boldsymbol{\Phi} \boldsymbol{V} - \boldsymbol{q}||_2^2 + \lambda ||\boldsymbol{V}||_1 \tag{6.5}$$

with λ being a regularisation parameter that controls the weight given to the regularisation term. Using l_2 as a regularisation term would result in a unique analytical solution, but l_1 is used despite not giving a unique solution. This is because the l_1 term promotes sparsity, meaning that several ECIs are set to zero, effectively choosing a subset of ECIs which prove to be the most relevant. As mentioned, this influences the computational cost of MC simulations later on.

To evaluate the predictive power of the cluster expansion produced, the leave-one-out cross validation score is used (LOOCV). It is defined as

$$\text{LOOCV} = \left(\frac{1}{N} \sum_{i=1}^{N} (\hat{q}_i - q_i)^2 \right)^{1/2} \tag{6.6}$$

where N is the number of configurations in the training set, q_i is a beforehand calculated physical quantity of a configuration i in the set. $\hat{q}_i$ is the same physical quantity, but predicted by CE using $N-1$ configurations, leaving out configuration i. This ensures that a prediction for a configuration is not directly influenced by the configuration it is predicting. In addition to evaluation of the predictive power, LOOCV allows for comparison between different setups for a cluster expansion.

In this thesis, the physical quantity of interest is the energy. With a set of ECIs and their corresponding clusters, the energy calculation for a specific configuration can be done with orders of magnitude less computational cost than with DFT. For calculation of the energy of a configuration eq. 5.7 becomes

$$E(\boldsymbol{\sigma}) = \sum_{\alpha} V_\alpha \Phi_\alpha \tag{6.7}$$

where all symmetrically equivalent clusters are classified as the same cluster, and this set of equivalent clusters is represented by α. More explicitly, it can be written as

$$E(\boldsymbol{\sigma}) = J_0 + \sum_{\alpha} m_\alpha J_\alpha \Phi_\alpha \tag{6.8}$$

where J_0 is the ECI of a cluster of size zero, effectively being a constant. m_α is the number of times the symmetrically equivalent clusters α occur and J_α is the ECI per occurrence. Simply put, energy calculations using CE is to count the number of times a specific cluster occurs, multiply it by an energy corresponding to that cluster and add it to the total energy.

6.4 Monte Carlo Simulations with CEMC

Having obtained a CE model of clusters and ECIs, Monte Carlo simulations can be performed in the canonical ensemble. For this, the package CEMC [15] is used, which performs Markov Chain Monte Carlo simulations with the Metropolis-Hastings algorithm [13][16]. The method requires numerous calculations of the total energy of a bulk of atoms, and the speed of the calculations with the CE model is what makes Monte Carlo simulations viable. The method for the canonical ensemble can be described as follows: The energy of a starting structure is calculated. Then, two atoms of different types are swapped and the energy of the new structure is calculated. The new configuration is kept with an acceptance probability

$$P = \min \left[1, \exp \left(\frac{-(E_{new} - E_{old})}{k_B T} \right) \right] \tag{6.9}$$

or else reverted to the previous. This constitutes one Monte Carlo step. After a sufficient amount of steps, the structure is in equilibrium at the given temperature.

For these simulations in the canonical ensemble, the composition of atoms is constant. To do simulations in the grand canonical ensemble, a slightly different approach is used to allow for changes to the composition. Instead of swapping two different atoms, the type of a single atom is swapped, and the new configuration is either kept or reverted to the previous one with the same probability P. The chemical potential μ is simulated by subtraction μ from the ECI of the one-body cluster. This allows for a changing composition, but the number of atoms is still constant. These simulations are therefore said to be in the semi-grand canonical ensemble.

Chapter 7

Results and Discussion

First, several calculations on both hcp and bcc structures of pure titanium are performed to evaluate and validate the execution of the DFT calculations. Then, a CE model is developed for hcp titanium-aluminium and further used in Monte Carlo simulations.

7.1 Convergence Tests

Before doing calculations on physical attributes, it is important to find out what values the GPAW parameters should have for the simulations to get accurate results. For this, a convergence test was done for the cutoff energy and the number of k-points. By calculating the energy for increasing values of these two parameters on a bcc titanium structure, the convergence of the energy can be visualised. This is shown for cutoff energy in figure 7.1 and k-points in figure 7.2. Based on these results, the standard parameters for the simulations done with 64 atoms were set to $k = 4$ and $E_{cut} = 600$ eV. It should be mentioned that for most calculations, the absolute value of the energy per atom is of less interest as DFT calculations tend to systematically over- or underestimate the energy depending on what parameters and exchange-correlation functionals are used. It is the energy relative to other simulations with similar parameters that give the most meaningful results. Figure 7.2 is also demonstrating how smaller

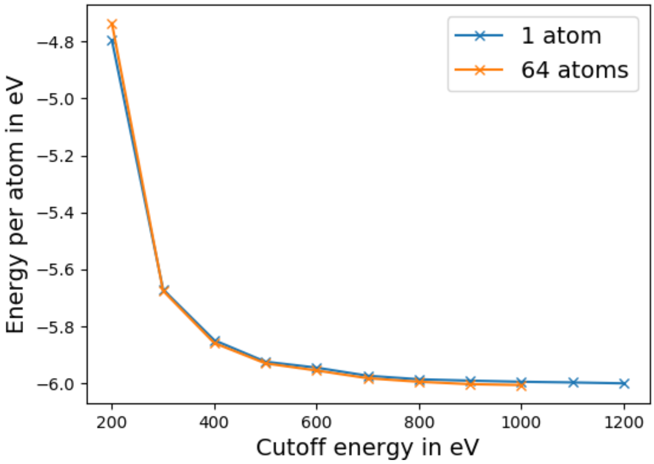

Figure 7.1: Convergence of energy per atom as the cutoff energy is increased. These calculations are done with 10 k-points in each dimension.

systems are more sensitive to the Brillouin zone sampling as mentioned in 6.2. The same convergence test was carried out for hcp titanium and yielded similar results.

7.2 Lattice Constants

A fundamental physical property of titanium is the lattice constant. As titanium can have two different structures, the lattice constants for both are calculated. Two different methods are exhibited. The method chosen for bcc is to calculate the total energy of 64 atoms in a given structure at different lattice constants. The number that gives the lowest total energy is then the lattice constant for the material according to the DFT simulations. The results from the bcc calculations are shown in figure 7.3. In this case, each data point takes about 1-2 hours to compute on one node with 20 processors, to give a sense of the time-scale of these simulations. By using polynomial interpolation, the lowest energy is found to occur at $a = 3.26$ Å.

For hcp titanium, the method used is to optimise the structure by relaxing

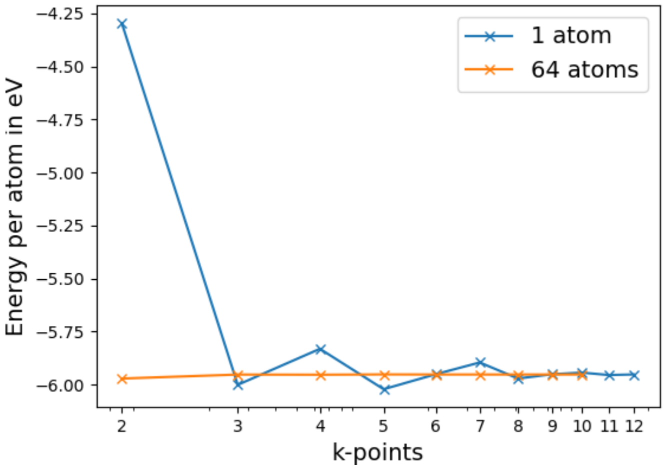

Figure 7.2: Convergence of the energy per atom with an increasing number of k-points. On the x-axis, the number of k-points represents one dimension. The total number of k-points is therefore N^3 and $E_{cut} = 600$ eV. The 64-atom simulation converges very quickly, while the single atom is unstable at lower values of k-points. They converge to the same energy.

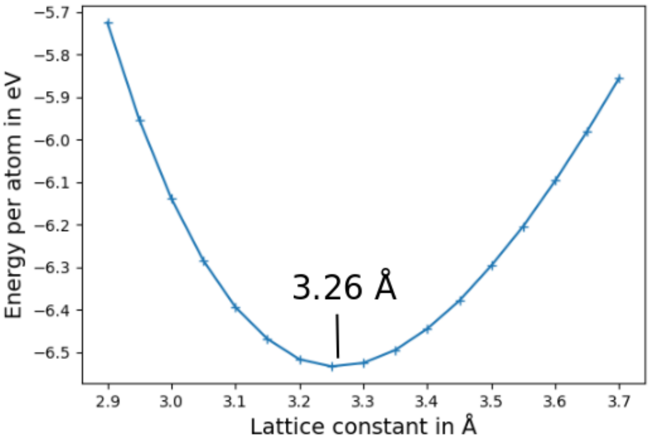

Figure 7.3: Simulating 64 titanium atoms in bcc structure for different lattice constants. The lowest energy is the lattice constant according to these simulations.

it. After using GPAW to calculate the force on every atom and the stress in the structure, an ASE algorithm is used to move the atoms towards what is likely to be a lower energy state. This relaxing process is reiterated until maximum force and stress are below a set limit[1]. The lattice constants of the optimised structure are listed in 7.1.

Table 7.1: The calculated lattice constants for hcp titanium compared to the correct value [3, p. 20].

Lattice constant	**Experimental**	**Calculated**
a	2.95 Å	2.938 Å
c	4.68 Å	4.648 Å

Both values are slightly below the experimental value, but the listed values are for room temperature and the calculations are done at absolute zero. The experimental values should therefore be viewed as an upper bound, due to thermal expansion. The ratio between the lattice constants is 1.582 compared to 1.633 for the ideal ratio for hcp, meaning that the AB stacking layers are closer together in the optimised structure. The experimental value for the ratio is 1.587 [**titianium**], meaning that the shape of the hcp structure is accurately calculated by DFT. The lowest energy per atom for bcc in figure 7.3 is -6.53 eV while for the hcp calculations it is -6.65 eV per atom. This indicates that hcp is the preferred configuration of titanium atoms at absolute zero temperature, which is in accordance with experimental results [17]. Only at temperatures above 1150 K does bcc become the preferred structure of pure titanium.

7.3 Electronic Band Structure

The band structure of both bcc and hcp titanium was calculated with GPAW. The results are shown in figure 7.4 and 7.5, along with the density of states.

---

[1] The algorithm used is LBFGS and the relaxation limits are set to 0.025 eVÅ^{-1} for force and 0.003 eVÅ^{-3} for stress.

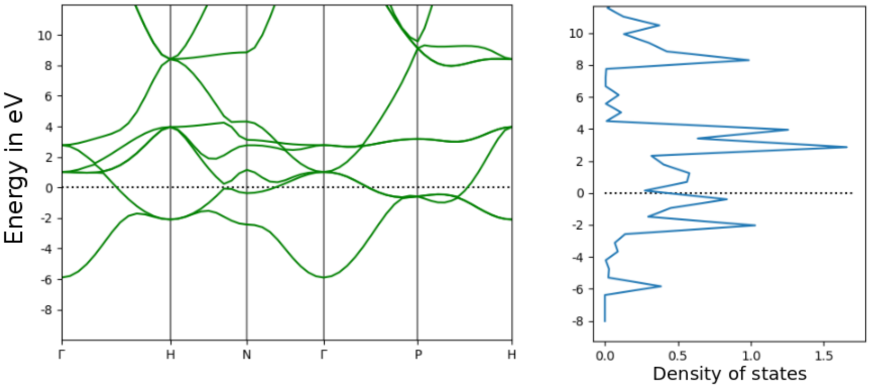

Figure 7.4: Band structure for bcc titanium. As expected for a metal, the bands cross over the Fermi level.

There are no band gaps at the Fermi level, as is expected with a metal. The band structures are close to identical to results found in another study [18].

7.4 Cohesive Energy

To find the cohesive energy, two energy calculations are needed. One for an atom in free space and one for an atom in a crystal structure. The GPAW mode is set to plane wave which requires a unit cell with periodic boundary conditions, meaning that to simulate an atom in free space, the unit cell would have to be of infinite size. Fortunately, interatomic forces reduce dramatically as distance increases, so the unit cell only has to be sufficiently large for an atom to experience free space. By increasing the lattice constant, the energy can be found by seeing what it converges to. Figure 7.6 shows this for a bcc structure, though the energy in interest is independent of the structure in this case. The energy converges towards -1.51 eV, which is used as the energy of a titanium atom in free space in further calculations.

For an atom in an hcp crystal, a bulk of 64 atoms is relaxed with periodic boundary conditions and the energy is calculated. The cohesive energy is then calculated with equation 2.9 and is found to be 5.14 eV. This is 6% greater

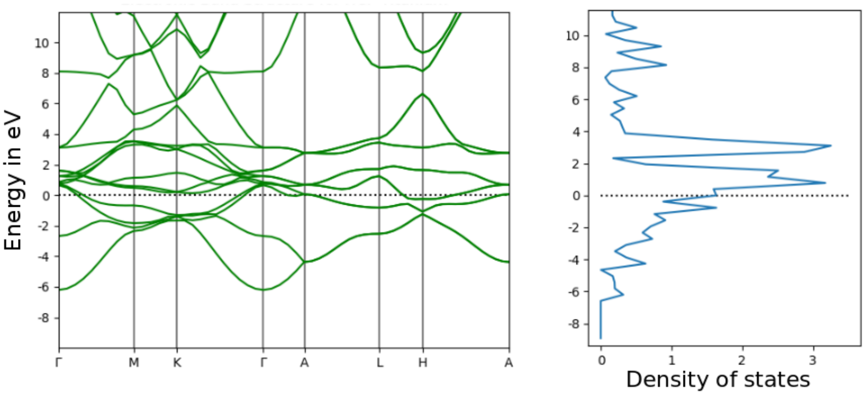

Figure 7.5: Bandstructure for hcp titanium. It has more bands close to the fermi level than its bcc counterpart.

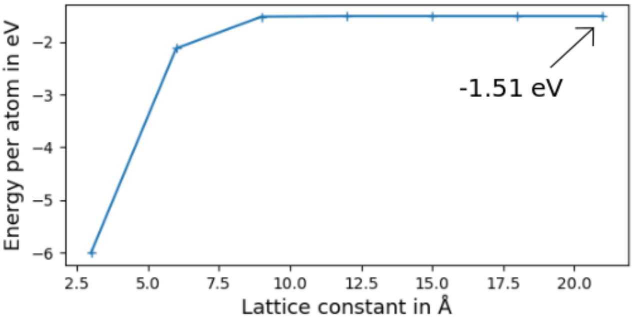

Figure 7.6: Energy of a single titanium atom. As the size of the unit cell increases, the energy quickly converges towards the energy of an atom in free space.

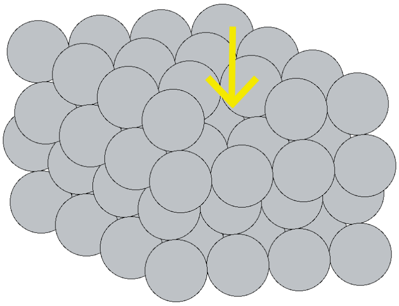

Figure 7.7: The 63 atom structure used for finding the vacancy formation energy. The yellow arrow shows the location of the vacancy.

than the experimentally found value of 4.85 eV [3, p. 50]. As mentioned, DFT's strength lies not in accurate predictions of real-world energies, but rather in the comparison between calculations performed with the same parameters. In this regard, a 6% overestimation can be viewed as an acceptable result.

7.5 Vacancy Formation Energy

To calculate the vacancy formation energy, a simulation of a crystal with a missing atom has to be carried out. To accomplish this, a bulk of 64 atoms in hcp configuration is again set up, but then one atom is removed, shown in figure 7.7. Because of the periodic boundary conditions, this means that the crystal simulated will be one with periodic vacancies. There are only three atoms between the vacancies, and this should be considered as a source of error. The bulk is optimised in the same way as for the lattice constant calculations. The optimisation ensures that the structure resembles what an actual vacancy would look like, instead of just being an artificial hole on the lattice. The optimised structure with 63 atoms has a total energy of -416.6 eV while the value for its optimised 64 atom counterpart is -425,4 eV. By equation 2.10, this gives a vacancy formation energy of 2.21 eV. Results for other studies are around 2.13-2.14 eV [19][20].

This concludes the benchmark testing of the DFT calculations and what follows is the study of the titanium-aluminium alloy.

7.6 Optimising Structures for Cluster Expansion

To construct a CE model for the titanium-aluminium alloy, several energy calculations with DFT are needed. The process is started by setting up hcp titanium structures of size $3 \times 3 \times 2$ unit cells (36 atoms) and changing atoms at random sites into aluminium. This way, random configurations of titanium-aluminium are constructed with a varying composition set to 0 - 50% aluminium, as this will be the range of interest in this thesis. The structures are then optimised like during the lattice constant and vacancy formation calculation until the maximum force and stress of the structure are below 0.025 $\text{eV}\text{Å}^{-1}$ and 0.003 $\text{eV}\text{Å}^{-3}$ respectively. All structures are relaxed to the same limits so that they are comparable to each other. Relaxing the structures effectively reduces the pressure to zero, meaning that the equation for enthalpy of formation (2.13) is valid. Using high-performance computing resources[2], 64 structures were successfully optimised, hereafter referred to as the training set.

7.7 Cluster Expansion

The optimised structures are used as the training set for a cluster expansion, which is evaluated in figure 7.8. The circles represent energies for a specific configuration as calculated by DFT and predicted by the CE. Ideally, they are located at the line, meaning that the CE predictions are accurate. The red circles are predictions with the leave-one-out method, while the blue circles' training sets include the structure being predicted. The figure shows that the accuracy, in general, is satisfactory, with some predictions being slightly off. The LOOCV score of 7.5 MeV/atom is similar to scores achieved in relatable studies [21][22].

---

[2] The resource used is the computer named "Stallo" at The Arctic University of Norway located in Tromsø.

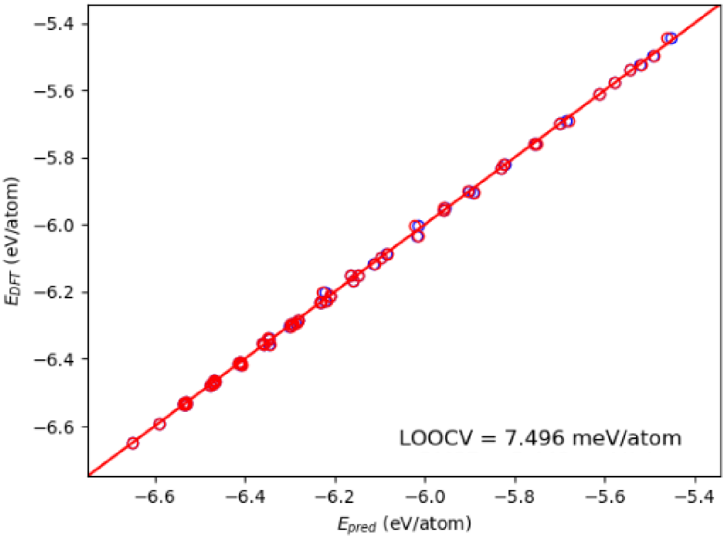

Figure 7.8: An evaluation of the CE predictions compared to the DFT calculations for all structures in the training set.

The cluster expansion is further evaluated in figure 7.9, showing the enthalpy of formation[3] from the DFT calculations of every structure together with the CE predictions. The important observations in this figure are at what concentrations there is a point on the black line, as this is likely to be a preferred crystal structure. Ideally, all CE predictions would be at the DFT value, but as the average energy per atom in the alloy ranges from -3.8 eV and -6.6 eV, most predictions are within 1% of the DFT value. As mentioned in section 6.3, a perfect fit is possible, but at the cost of a much more computationally expensive CE model and possible overfitting.

The effective cluster interactions are shown in figure 7.10. The clusters are named $cX_1\_X_2nn\_X_3$ after how many atoms they consist of, maximum nearest neighbour distance in the cluster and an identification number to separate clusters sharing the two first classifications. The zero and one atom clusters dominate, but are not of much interest as they do not dictate what crystal

---

[3] The numerical values on the y-axis is not comparable to later results since calculation of the enthalpy of formation arbitrarily includes the highest energy of the structures at 50% as a reference point.

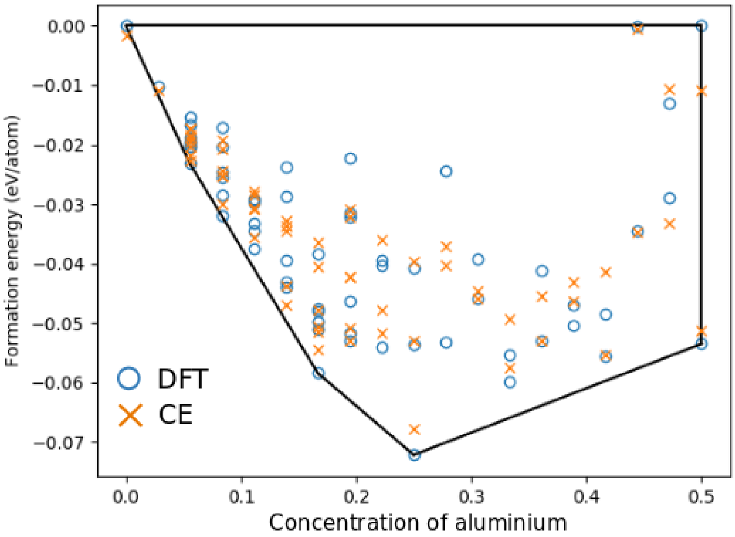

Figure 7.9: The DFT energies for the structures alongside the CE predictions plotted as enthalpy of formation. The points on the black line indicate favourable structures at that concentration.

structures might form. Figure 7.11 shows the ECIs without the two first values so that the remaining values are distinguishable. The two-body, nearest neighbour cluster has a positive value. This means that the configuration $\boldsymbol{\sigma}$ (5.1) of two atoms of the same element gives a positive contribution to the total energy, while two different atoms next to each other will reduce it. From this, it can be understood that titanium and aluminium are prone to form an alloy, as any mixture where atoms of the two elements neighbour each other will lower the total energy.

A selection of the most influential clusters is shown in figure 7.12. The clusters of higher body count are harder to interpret, but dictate what type of crystal structure is the most energetically beneficial. In this CE the configuration variable σ_i is 1 for aluminium and -1 for titanium. As an example, the three body structure of figure 7.12 is considered. With its positive ECI, three aluminium atoms in this configuration would give a positive energy contribution, while three titanium atoms would be energetically favourable. Furthermore, two aluminium and one titanium would have a negative contribution, while

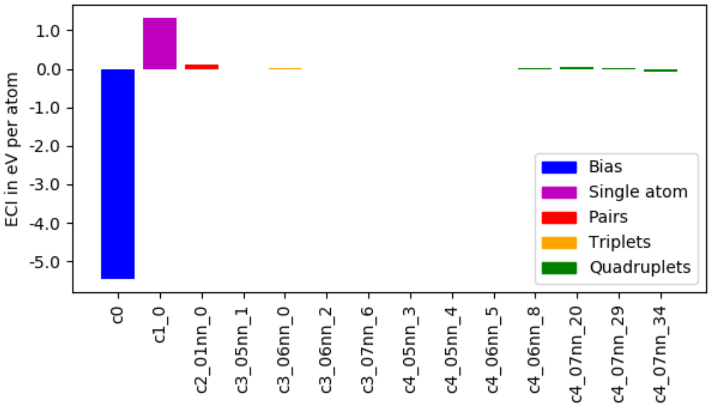

Figure 7.10: The effective cluster interactions for each cluster in the model. Evidently, the zero and one atom cluster dominate.

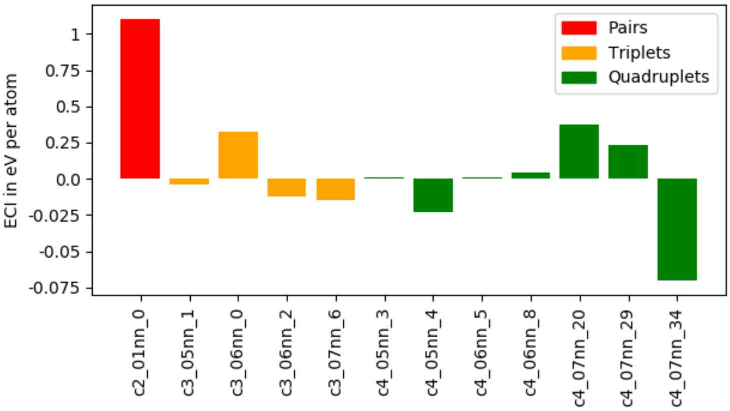

Figure 7.11: ECIs without the zero and one atom cluster.

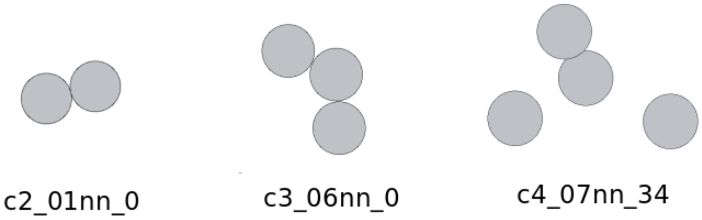

Figure 7.12: A selection of the most influential clusters.

two titanium and one aluminium would contribute positively.

7.8 Monte Carlo Simulations

With the obtained cluster expansion model, Monte Carlo simulations are executed in both the canonical and the semi-grand canonical ensemble.

7.8.1 Canonical Ensemble

Two thousand atoms are set up in a structure of 10 × 10 × 10 hpc unit cells and cooled down in the canonical ensemble for varying concentrations of aluminium. The enthalpy of formation for titanium-aluminium up to 50% aluminium is shown in figure 7.13.

As deduced from the ECIs, titanium and aluminium lower their total energy if mixed. This is visible here as the energy steadily goes down as concentration moves towards 50%, even at higher temperatures. The phase diagram in figure 1.1 puts the highest temperature for the melting point at about 2000 K, so no energy fluctuations as a cause of configuration is expected above this temperature, since the atoms of a liquid are allowed to move freely. Therefore, the higher temperatures produce a smooth line. When lowering the temperature, the differences among the concentrations emerge. At 25% aluminium, there apparently exists a discontinuity in the slope. By investigating the structure for the lowest temperature at this concentration, shown in figure 7.14a, the crystal structure Ti3Al [23] is identified. Concentrations in the vicinity of 25%

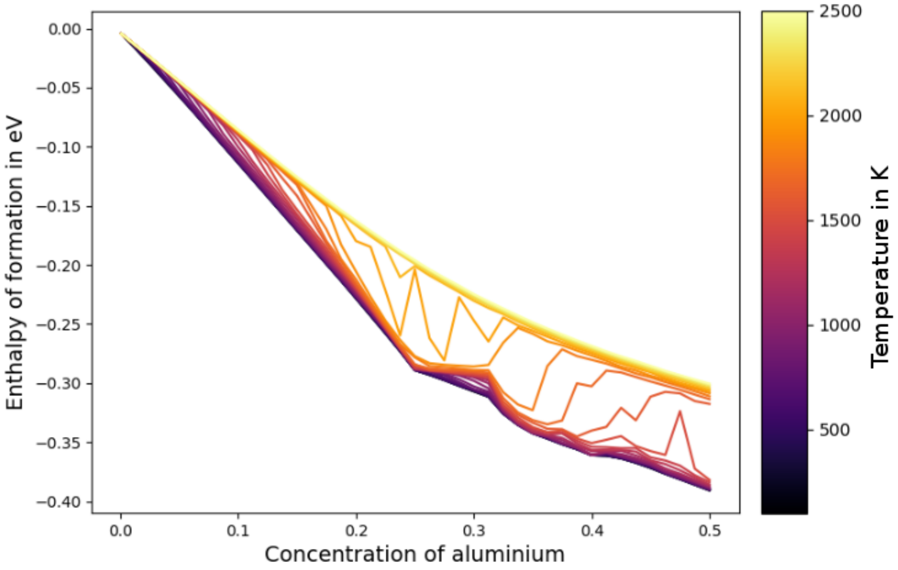

Figure 7.13: Enthalpy of formation for titanium-aluminium for a range of energies.

also produce this crystal structure, but then with domains of either pure titanium or aluminium depending on whether the concentration is lower or higher than 25%. This suggests that Ti3Al is a preferable configuration for the alloy. The cooled down structure at 50% aluminium is shown in figure 7.14b. This bulk does not have a perfectly ordered structure, though AB stacking is seen in domains. When looking up the TiAl crystal [24], it is found to be in a bcc configuration, rather than hcp. The phase diagram in figure 1.1 shows that the TiAl phase starts at about 49% aluminium. As the CE model is trained on hcp structures, predictions for composition above 49% aluminium is like forcing the structure to stay hcp when it could lower its energy further by rearranging to bcc. This is likely to be the reason why the structure in 7.14b is not perfectly ordered.

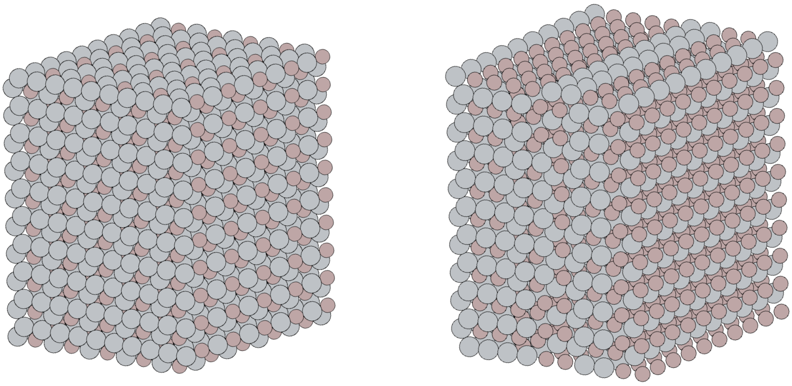

(a) Ti3Al crystal at 25% Al. **(b)** 50% concentration of aluminium.

Figure 7.14: Visualisation of the bulk at 25% and 50% concentration at 100 K from the calculations shown in figure 7.13.

7.9 Grand Canonical Ensemble

Similarly to in the canonical ensemble, a bulk of 2000 atoms is cooled down. Here, the concentration of aluminium is allowed to change, while the chemical potential is kept constant. Figure 7.15 shows this process for a range of chemical potentials from 0.94 to 1.16 eV/atom. The figure shows stable phases at 0%, 25% and 50%. All simulations that end up at 25% are in the same crystal structure as shown in figure 7.14a.

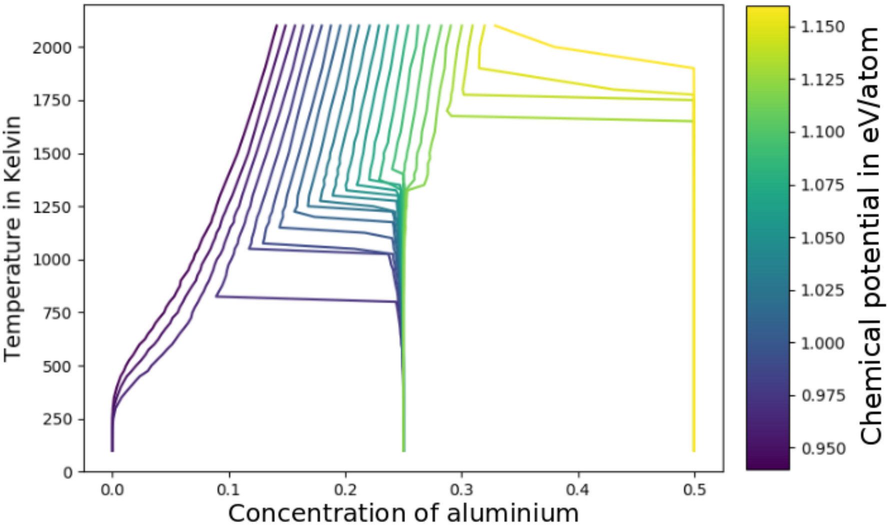

Figure 7.15: Cooling down structures at different, constant chemical potentials.

Chapter 8

Conclusion

The titanium-aluminium alloy in hcp configuration has been studied. Initially, DFT calculations were performed for verification of their validity. Input parameters for the GPAW calculator that produced convergent results were found, and several physical properties were computed for pure titanium. Lattice constants, electronic band structures, cohesive energy and vacancy formation energy were all in agreement with results from other sources. DFT was used to calculate the energies of a set of structures with varying composition of titanium and aluminium. This training set was then used to develop a CE model, which had an acceptable LOOCV score of 7.5 MeV/atom. With this CE model, Monte Carlo simulations were done for a bulk of 2000 atoms in both the canonical and the semi-grand canonical ensemble. The Ti3Al crystal was identified as a preferable structure at concentrations around 25%. Closer to 50%, the validity of the CE model becomes questionable, and a stable TiAl structure on a hcp lattice was not found.

It is seen that density functional theory can give results that accurately describe reality, given the right parameters. Furthermore, Monte Carlo simulations based on a cluster expansion of DFT calculations is proven to give valid representations of alloy structures under the right circumstances.

Chapter 9

Future Work

As a continuation of the Monte Carlo simulations, nucleation phase boundaries for the Ti3Al structure could be calculated, both from the pure titanium side and the TiAl side. Another interesting topic of study is titanium grade 5, which in addition to aluminium contains vanadium, and is a well known titanium alloy. The vanadium acts as a bcc-stabiliser that together with the hcp-stabilising aluminium creates an alloy with domains of both structures.

Bibliography

[1] Dr. Christoph Leyens Dr. Manfred Peters. *Titanium and Titanium Alloys: Fundamentals and Applications.* Wiley-VCH Verlag GmbH Co. KGaA, 2003.

[2] *Interdiffusion Behavior of Aluminide Coated Two-Phase 2-Ti3Al/-TiAl Alloys at High Temperatures - Scientific Figure on ResearchGate.* URL: `https://www.researchgate.net/figure/Equilibrium-phase-diagram-of-Ti-Al-6_fig1_312642630%20[accessed%2017%20Jun,%202019]`.

[3] Charles Kittel. *Introduction to Solid State Physics.* 8th ed. John Wiley Sons, Inc, 2005.

[4] Gerald D. Mahan. “Crystal”. In: *Encyclopædia Britannica, inc.* (Oct. 2012).

[5] O Le Bacq, Francois Willaime, and Alain Pasturel. “Unrelaxed vacancy formation energies in group-IV elements calculated by the full-potential linear muffin-tin orbital method: Invariance with crystal structure”. In: *Phys. Rev. B* 59 (Apr. 1999).

[6] Jens 0. Andersen. *Introduction to Statistical Mechanics.* 1st ed. Akademika forlag, 2014.

[7] Robert G Parr. *Density-Functional Theory of Atoms and Molecules.* eng. New York: Oxford University Press, 1995. ISBN: 1-280-52770-6.

[8] C. David Sherrill. “An Introduction to Hartree-Fock Molecular Orbital Theory”. In: (2000).

[9] R. M. Martin. *Electronic Structure. Basic Theory and Practical Methods.* Cambridge University Press, 2004.

[10] William L. Dunn and J. Kenneth Shultis. “1 - Introduction”. In: *Exploring Monte Carlo Methods.* Ed. by William L. Dunn and J. Kenneth Shultis. Amsterdam: Elsevier, 2012, pp. 1–20. ISBN: 978-0-444-51575-9. DOI: `https://doi.org/10.1016/B978-0-444-51575-9.00001-4`.

[11] Ask Hjorth Larsen et al. “The atomic simulation environment—a Python library for working with atoms”. In: *Journal of Physics: Condensed Matter* 29.27 (2017), p. 273002.

[12] P. E. Blöchl. “Projector augmented-wave method”. In: *Phys. Rev. B* 50 (24 Dec. 1994), pp. 17953–17979. DOI: `10.1103/PhysRevB.50.17953`. URL: `https://link.aps.org/doi/10.1103/PhysRevB.50.17953`.

[13] Jin Hyun Chang et al. “CLEASE: A versatile and user-friendly implementation of Cluster Expansion method”. In: *arXiv e-prints*, arXiv:1810.12816 (Oct. 2018), arXiv:1810.12816. arXiv: `1810.12816 [cond-mat.mtrl-sci]`.

[14] Lance J. Nelson et al. “Compressive sensing as a paradigm for building physics models”. In: 87.3, 035125 (Jan. 2013), p. 035125. DOI: `10.1103/PhysRevB.87.035125`. arXiv: `1208.0030 [cond-mat.mtrl-sci]`.

[15] David Kleiven. *Monte Carlo package targeted at systems studied with the Cluster Expansion.* 2019. URL: `https://github.com/davidkleiven/CEMC`.

[16] Siddhartha Chib and Edward Greenberg. “Understanding the Metropolis-Hastings Algorithm”. In: *The American Statistician* 49.4 (1995), pp. 327–335. ISSN: 00031305. URL: `http://www.jstor.org/stable/2684568`.

[17] Julius C. Schuster and Martin Palm. “Reassessment of the binary Aluminum-Titanium phase diagram”. In: *Journal of Phase Equilibria and Diffusion* 27.3 (June 2006), pp. 255–277. ISSN: 1863-7345.

[18] Mahmoud Jafari and Hamid reza Hajiyani. "Optical properties of , and structure of Titanium: Ab initio approach". In: *Computational Materials Science* 50.9 (2011), pp. 2549–2553. ISSN: 0927-0256.

[19] O. Le Bacq, F. Willaime, and A. Pasturel. "Unrelaxed vacancy formation energies in group-IV elements calculated by the full-potential linear muffin-tin orbital method: Invariance with crystal structure". In: *Phys. Rev. B* 59 (13 Apr. 1999), pp. 8508–8515. DOI: `10.1103/PhysRevB.59.8508`. URL: `https://link.aps.org/doi/10.1103/PhysRevB.59.8508`.

[20] B. Drittler et al. "Vacancy formation energies of fcc transition metals calculated by a full potential green's function method". In: *Solid State Communications* 79.1 (1991), pp. 31–35. ISSN: 0038-1098. DOI: `https://doi.org/10.1016/0038-1098(91)90474-A`. URL: `http://www.sciencedirect.com/science/article/pii/003810989190474A`.

[21] David Kleiven et al. "Atomistic simulations of early stage clusters in AlMg alloys". In: *Acta Materialia* 166 (2019), pp. 484–492. ISSN: 1359-6454. DOI: `https://doi.org/10.1016/j.actamat.2018.12.050`. URL: `http://www.sciencedirect.com/science/article/pii/S1359645418310012`.

[22] Manh Cuong Nguyen et al. "Cluster expansion modeling and Monte Carlo simulation of alnico 5–7 permanent magnets". In: *Journal of Applied Physics* 117.9 (2015), p. 093905. DOI: `10.1063/1.4914036`. eprint: `https://doi.org/10.1063/1.4914036`. URL: `https://doi.org/10.1063/1.4914036`.

[23] Pierre Villars and Karin Cenzual, eds. *Ti3Al Crystal Structure: Datasheet from "PAULING FILE Multinaries Edition – 2012" in SpringerMaterials (https://materials.springer.com/isp/crystallographic/docs/sd_1210830)*. accessed 2019-06-17. URL: `https://materials.springer.com/isp/crystallographic/docs/sd_1210830`.

[24] Pierre Villars and Karin Cenzual, eds. *TiAl Crystal Structure: Datasheet from "PAULING FILE Multinaries Edition – 2012" in SpringerMaterials (https://materials.springer.com/isp/crystallographic/docs/sd_0532461)*. ac-

cessed 2019-06-17. URL: `https://materials.springer.com/isp/crystallographic/docs/sd_0532461`.

NTNU
Norwegian University of
Science and Technology